Kinematic wave model of bed profiles in alluvial channels

Gokmen Tayfur[1] and Vijay P. Singh[2]

Received 7 March 2005; revised 23 February 2006; accepted 10 March 2006; published 21 June 2006.

[1] A mathematical model, based on the kinematic wave (KW) theory, is developed for describing the evolution and movement of bed profiles in alluvial channels. The model employs a functional relation between sediment transport rate and concentration, a relation between flow velocity and depth and Velikanov's formula relating suspended sediment concentration to flow variables. Laboratory flume and field data are used to test the model. Transient bed profiles in alluvial channels are also simulated for several hypothetical cases involving different water flow and sediment concentration characteristics. The model-simulated bed profiles are found to be in good agreement with what is observed in the laboratory, and they seem theoretically reasonable for hypothetical cases. The model results reveal that the mean particle velocity and maximum concentration (maximum bed form elevation) strongly affect transient bed profiles.

Citation: Tayfur, G., and V. P. Singh (2006), Kinematic wave model of bed profiles in alluvial channels, *Water Resour. Res.*, *42*, W06414, doi:10.1029/2005WR004089.

1. Introduction

[2] Because of its ubiquitous importance, transmission of sediment waves (evolution of bed profiles) in alluvial channels has been extensively studied both experimentally and mathematically. Experimental studies have involved extensive flume and field observations [e.g., *Guy et al.*, 1966; *Langbein and Leopold*, 1968; *Soni*, 1981a; *Wathen and Hoey*, 1998; *Lisle et al.*, 1997, 2001]. Also, extensive experimental, theoretical, and numerical modeling work has been done to investigate transmission of sediment waves in mountain gravel bed rivers where sediment waves or pulses can form following variations in input from landslides, debris flows, and other sources [*Cui et al.*, 2003a, 2003b, 2005; *Cui and Parker*, 2005].

[3] Flume experiment and field studies have enhanced our understanding of basic mechanisms of bed formation and bed movement in alluvial channels. Considerable effort has been devoted to developing theoretical models for predicting bed profiles in alluvial channels. These models have ranged from simple conceptual representations of transport in uniform flow in clear water [*Vreugdenhil and de Vries*, 1973; *de Vries*, 1973] to comprehensive representations treating transport in sediment laden nonuniform and unsteady flow and considering the interaction between suspended sediment and movable bed layer [*Pianese*, 1994]. These models are either diffusion wave [e.g., *de Vries*, 1973; *Soni*, 1981b; *Ribberink and Van Der Sande*, 1985; *Lisle et al.*, 2001] or dynamic wave [e.g., *Ching and Cheng*, 1964; *Vreugdenhil and de Vries*, 1973; *Ribberink and Van Der Sande*, 1985; *Pianese*, 1994; *Cao and Carling*, 2003] for simulating evolution of bed profiles.

[4] In these diffusion and dynamic wave models different sediment transport functions have been employed. *Hotchkiss and Parker* [1991] related sediment transport rate to grain shear stress while in other studies transport rate is mostly related to flow variables using power law [*de Vries*, 1965; *Vreugdenhil and de Vries*, 1973; *Mahmood*, 1975; *Philips and Sutherland*, 1983; *Ribberink and Van Der Sande*, 1985; *Cao and Carling*, 2003]. *Gomez and Church* [1989] and *Yang and Wan* [1991] discussed the performance of commonly used sediment transport functions in simulating evolution of bed profiles in alluvial channels.

[5] Review of literature shows that the sediment transport function has been expressed as a function of water flow variables and the bed formation and bed movement have been treated as having diffusion wave characteristics. However, through experimental studies, *Langbein and Leopold* [1968] showed that the evolution and movement of bed profiles can be treated as kinematic wave, exhibiting a functional relation between sediment transport rate and concentration. They carried out 11 flume experiments on individual particles (glass spheres) [4.7 mm in diameter] moving in a narrow flume [width = 7 cm] under the traction of water flow. They observed that the particles did not move uniformly but formed groups rather quickly. Closely spaced particles traveled slower than did widely spaced particles. As the rate of particle feed was increased, the size of groups increased and the average speed decreased so that ultimately all motion halted. Analyzing the experimental data, they found that there was a strong relation between transport rate and concentration. They extended their analysis to sand transport in pipes and flumes. Analyzing the experimental data of *Blatch* [1906], *Howard* [1939] and *Durand* [1953] on sand movement in pipes and experimental data of *Guy et al.* [1966] on sand movement in flumes, *Langbein and Leopold* [1968] observed that the sand movement in pipes and flumes behaved similarly as the movement of glass spheres (beads) and there existed flux-concentration curves for sand flow in pipes and sand flow in flumes, similar to the case of beads. They further extended their analysis to

[1]Department of Civil Engineering, Izmir Institute of Technology, Gulbahce Kampus, Urla, Izmir, Turkey.
[2]Department of Biological and Agricultural Engineering, Texas A & M University, College Station, Texas, USA.

0043-1397/06/2005WR004089$09.00

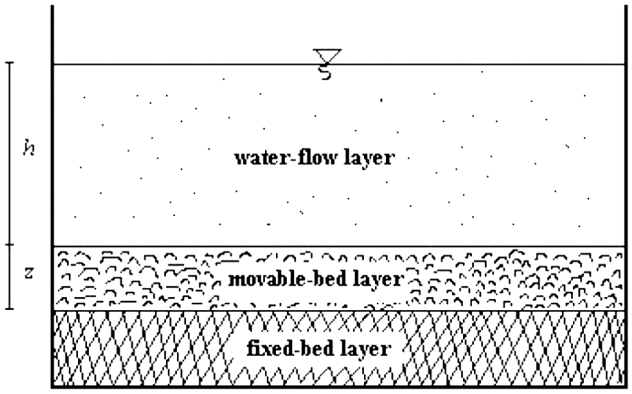

Figure 1. Schematic representation of two-layer system.

gravel and cobble bars spaced along the length of ephemeral streams of Santa Fe River. By placing rocks on the streambed in groups with varying spacing between individual cobbles, they observed that rocks in groups having wider spacing moved more readily than did rocks that were close together. They observed a similar type of transport rate-concentration relationship. These flux-concentration curves, however, differed greatly from those of water waves. For example, the flux-concentration relation for water waves in channel shows increasing velocity for increasing concentration (flow depth). On the other hand, in bead, sand, and rock experiments, particles interact and their mean speed decreases with increasing concentration.

[6] Although laboratory and field data of *Langbein and Leopold* [1968] provide strong evidence that the evolution and movement of bed profiles can be described by the kinematic wave theory, little has since been done. Their discussion is primarily conceptual and the mathematical formulation is yet to be developed.

[7] The objective of this study is to develop a mathematical model, using the kinematic wave theory, for describing the bed profile evolution and movement in alluvial channels and to test the model against measured flume and laboratory data. Another objective is to evaluate the model by simulating bed profiles for several hypothetical scenarios and examine if these simulated bed profiles are theoretically reasonable.

2. Mathematical Development

[8] The bed profile evolution and movement in alluvial channels can be represented as a system involving two layers: water flow layer and movable bed layer, as shown in Figure 1. The flow layer may contain suspended sediment. The movable bed layer consists of water and sediment particles and therefore has porosity. For a wide rectangular alluvial channel with both layers, the conservation of mass equations for water and sediment on a unit width can be written as:

$$\frac{\partial h(1-c)}{\partial t}+\frac{\partial hu(1-c)}{\partial x}+(1-p)\frac{\partial z}{\partial t}+\frac{\partial q_{bw}}{\partial x}=q_{lw} \qquad (1)$$

$$\frac{\partial hc}{\partial t}+\frac{\partial huc}{\partial x}+p\frac{\partial z}{\partial t}+\frac{\partial q_{bs}}{\partial x}=q_{ls} \qquad (2)$$

where h = the flow depth (L); u = the flow velocity (L/T); c = the volumetric sediment concentration in the water flow phase (in suspension) (L^3/L^3); z = the mobile bed layer elevation (L); q_{bw} = the water flux in the mobile bed layer (L^2/T); q_{lw} = the lateral water flux (L/T); x = the independent variable representing the coordinate in the longitudinal direction (flow direction) (L); t = the independent variable of time (T); p = volume of solids in unit volume of bed sediment (one minus porosity) (L^3/L^3); q_{bs} = the sediment flux in the movable bed layer (L^2/T); and q_{ls} = the lateral sediment flux (L/T).

[9] Simplified forms of equations (1) and (2) have been given by *Ching and Cheng* [1964], *Vreugdenhil and de Vries* [1973], *Mahmood* [1975], and *Pianese* [1994]. For example, *Vreugdenhil and de Vries* [1973] assumed a steady ($\partial h/\partial t = 0$) but nonuniform clear water flow (i.e., $c = 0.0$) in the water flow phase. *Ching and Cheng* [1964] and *Pianese* [1994] neglected the last terms on the left hand sides of equations (1) and (2). *Cao and Carling* [2003] assumed clear water (i.e., $c = 0$) and neglected, on the left hand side, the last term in equation (1) and second term in equation (2). One simplification common in almost all investigations is the omission of the last term on the left hand side of equation (1). This term represents the water flux gradient in the movable bed layer. Compared to the water flux gradient in the water flow layer, this term is small and is therefore also omitted in this study. Furthermore, if there is no lateral inflow of water and sediment to the channel reach, the terms on the right hand sides of equations (1) and (2) vanish.

[10] Equations (1) and (2) contain five unknowns: h, u, c, z, and q_{bs}, provided that q_{bw} is neglected. Thus three additional equations are needed. One equation is obtained from the momentum conservation for the water flow layer. While *Ching and Cheng* [1964] and *Pianese* [1994] employed the full dynamic wave equation, *de Vries* [1973], *Vreugdenhil and de Vries* [1973], *Ribberink and Van Der Sande* [1985] and *Cao and Carling* [2003] used simplified forms. In this study, the kinematic wave approximation is employed:

$$u=\alpha\, h^{\beta-1} \qquad (3)$$

where α is the depth discharge coefficient or the kinematic wave resistance parameter ($L^{0.5}/T$) [*Singh*, 1996] and β is exponent. Employing Chezy's equation for the friction slope, $\beta = 1.5$ and $\alpha = C_z S_f^{0.5}$, where C_z is the Chezy roughness coefficient ($L^{0.5}/T$), S_f = friction slope and is taken as equal to S_o = bed slope.

[11] Another equation is obtained by relating the volumetric concentration of sediments transported by water flow (c) to flow variables [*Ching and Cheng*, 1964; *de Vries*, 1965; *Lai*, 1991; *Pianese*, 1994]:

$$c=\delta u^{\eta} h^{\xi} \qquad (4)$$

where exponents δ, η, and ξ are functions of water flow and sediment characteristics. This study employed the equation of *Velikanov* [1954]:

$$c=\frac{\kappa u^3}{g v_f h} \qquad (5)$$

where κ is the coefficient of sediment transport capacity; g is the gravitational acceleration (L/T^2) and v_f is the average fall velocity of sediments (L/T). Comparison of equation (4) with equation (5) shows that $\delta = \kappa(gv_f)$, $\eta = 3$, and $\xi = -1$. Substituting equation (3) into equation (5), one obtains:

$$c = \delta\alpha^3 h^{3\beta-4} \tag{6}$$

[12] Finally, a fifth equation can be obtained by relating sediment transport rate (sediment flux) to sediment concentration in the movable bed layer. As pointed out earlier, previous investigations have related sediment flux in the movable bed layer to the mean water flow velocity in the water flow layer and used a complete or diffusion waveform of the momentum equation. In this study, the kinematic wave theory was, however, employed. To that end, *Langbein and Leopold* [1968] proposed a sediment flux-concentration relation:

$$q_{st} = v_s C_b \left[1 - \frac{C_b}{C_{b_{\max}}}\right] \tag{7}$$

where q_{st} = the sediment transport rate ($M/L/T$); v_s = the velocity of sediment particles as concentration approaches zero (L/T); C_b = the areal sediment concentration (M/L^2); and $C_{b\max}$ = the maximum areal sediment concentration when transport ceases (M/L^2).

[13] Equation (7) states that flux increases with concentration until it reaches a maximum value and then starts decreasing reaching zero when $C_b = C_{b\max}$. On the basis of the flume sediment transport experiments of *Guy et al.* [1966], *Langbein and Leopold* [1968] suggested a value of $C_{b\max} = 245$ kg/m^2.

[14] Note that sediment flux (q_{bs}) in equation (2) is defined in (L^2/T) and the transport rate (q_{st}) in equation (7) is defined in (M/L/T). Therefore one can relate both the variables as:

$$q_{st} = \rho_s q_{bs} \tag{8}$$

where ρ_s is the sediment mass density (M/L^3). Furthermore, the areal concentration (C_b) can be related to the bed elevation (z) as:

$$C_b = p\ z\ \rho_s \tag{9}$$

Substitution of equations (8) and (9) into equation (7) would result in the following equation relating sediment flux to bed elevation (sediment concentration):

$$q_{bs} = pv_s z\left[1 - \frac{z}{z_{\max}}\right] \tag{10}$$

where $z_{\max}$ is the maximum bed elevation (L). Note that the derivative of q_{bs} with respect to x is required in equation (2). This can be obtained by using the chain rule:

$$\frac{\partial q_{bs}}{\partial x} = pv_s\left[1 - \frac{2z}{z_{\max}}\right]\frac{\partial z}{\partial x} \tag{11}$$

[15] Equations (3), (6) and (11), together with equations (1) and (2), form the system of five equations for modeling the evolution and movement of bed forms in alluvial channels. Combining equations (3), (6), and (11) with equations (1) and (2), the system of equations, after algebraic manipulation, can be written in compact form as:

$$\left[1 - \eta\beta\alpha^3 h^{\beta-1}\right]\frac{\partial h}{\partial t} + \left[\alpha\beta h^{\beta-1} - \eta\beta\alpha^4 h^{2\beta-2}\right] \cdot \frac{\partial h}{\partial x} + (1-p)\frac{\partial z}{\partial t} = q_{lw} \tag{12}$$

$$\left[\eta\beta\alpha^3 h^{\beta-1}\right]\frac{\partial h}{\partial t} + \left[\eta(2\beta-1)\alpha^4 h^{2\beta-2}\right]\frac{\partial h}{\partial x} + p\frac{\partial z}{\partial t} + pv_s\left[1 - \frac{2z}{z_{\max}}\right]\frac{\partial z}{\partial x} = q_{ls} \tag{13}$$

Equations (12) and (13) represent kinematic wave equations for modeling channel bed formation and movement. The two processes of water flow and sediment transport are interlinked not only throughflow variables (h and u) but also the sediment particle velocity v_s which is a function of particle characteristics and flow variables. *Levy* [1957], *Sharmov* [1959] and *Gongcharov* [1962] suggested different relationships for v_s. *Chien and Wan* [1999] concluded that the Gongcharov formula is more appropriate for flows in flumes and rivers. For $0.08 < d_s < 10$ mm and $10 < h/d_s < 1550$, *Chien and Wan* [1999] presented the following relation:

$$v_s = u - \frac{(u_c/1.4)^3}{u^2} \tag{14}$$

where d_s = the particle diameter (L), and u_c = the critical flow velocity at the incipient sediment motion (L/T).

[16] Equation (14) expresses the particle velocity as a function of mean flow velocity. *Bridge and Dominic* [1984] and *Bridge and Bennett* [1992], on the other hand, expressed the particle velocity as a function of skin shear stress that is represented as a shear velocity (see Appendix A). As it is shown in Appendix A, both the formulations yield comparable performance. u_c is expressed as a function of the particle fall velocity (v_f) and the shear velocity Reynolds number (R^*) as [*Yang*, 1996]:

$$u_c = \begin{cases} \dfrac{2.5v_f}{log(R^*) - 0.06} + 0.66v_f & 1.2 < R^* < 70 \\ 2.05v_f & R^* > 70 \end{cases} \tag{15}$$

where the shear velocity Reynolds number is expressed as [*Yang*, 1996]:

$$R^* = \frac{u_* d_s}{\upsilon} \tag{16}$$

where υ = kinematic viscosity of water (L^2/T), and u_* is the shear velocity (L/T) and it is defined as [*Yang*, 1996]:

$$u_* = \sqrt{ghS_o} \tag{17}$$

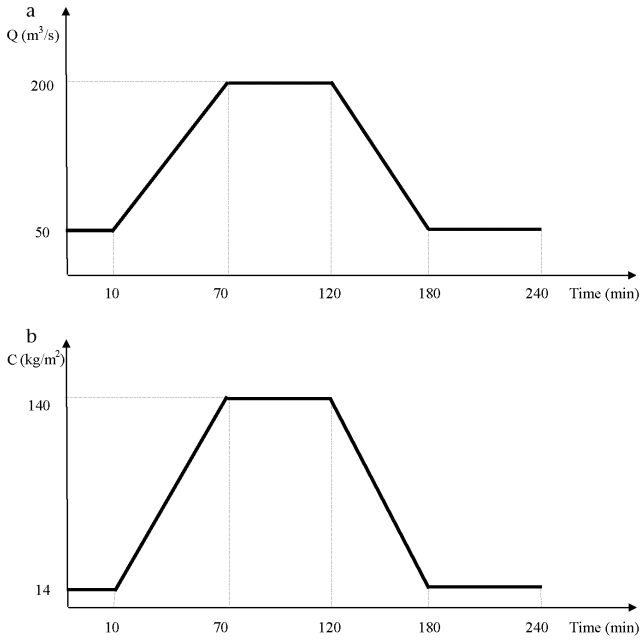

Figure 2. (a) Inflow hydrograph. (b) Inflow concentration.

When the particle Reynolds number ($R_{pn} = v_f d_s/\upsilon$) is less than 2.0, the fall velocity of a particle is expressed as [*Yang*, 1996]:

$$v_f = \begin{cases} \dfrac{1}{18}\dfrac{(\gamma_s - \gamma_w)}{\gamma_w}\dfrac{g d_s^2}{\upsilon} & d_s \le 0.1 \text{ mm} \\ F\left[\dfrac{g d_s(\gamma_s - \gamma_w)}{\gamma_w}\right]^{0.5} & 0.1 \text{ mm} < d_s \le 2.0 \text{ mm} \\ 3.32\sqrt{d_s} & d_s > 2.0 \text{ mm} \end{cases} \quad (18)$$

where γ_s = specific weight of sediment ($M/L^2/T^2$); γ_w = specific weight of water ($M/L^2/T^2$); and

$$F = \begin{cases} \left[\dfrac{2}{3} + \dfrac{36\upsilon^2\gamma_w}{g d_s^3(\gamma_s - \gamma_w)}\right]^{0.5} - \left[\dfrac{36\upsilon^2\gamma_w}{g d_s^3(\gamma_s - \gamma_w)}\right]^{0.5} & 0.1 \text{ mm} < d_s \le 1.0 \text{ mm} \\ 0.79 & 1.0 \text{ mm} < d_s \le 2.0 \text{ mm} \end{cases} \quad (19)$$

When the particle Reynolds number is greater than 2.0, the particle fall velocity is determined experimentally. *Yang* [1996] has given a figure summarizing the particle fall velocity values depending on the sieve diameter and the shape factor. For most natural sands, the shape factor is 0.7 and *Rouse* [1938] gave $v_f = 0.024$ m/s for $d_s = 0.2$ mm. In this study, for $R_{pn} > 2.0$, the particle fall velocity is assumed to be 0.024 m/s. Note that equation (18) is, in essence, valid for perfect spheres. *Dietrich* [1982] developed empirical functions that can consider the effect of shape and roundness on the particle fall velocity (see Appendix A). As it is shown in Appendix A, *Yang*'s [1996] formulation for particle fall velocity yields comparable results as that of *Dietrich* [1982].

[17] The kinematic wave equations for bed formation and movement (equations (12) and (13)) can be further simplified under certain conditions. For example, under the clear water assumption $c = 0$ and consequently parameter $\eta = 0$ in equations (12) and (13). Therefore

$$\frac{\partial h}{\partial t} + \alpha\beta h^{\beta-1}\frac{\partial h}{\partial x} + (1-p)\frac{\partial z}{\partial t} = q_{lw} \quad (20)$$

$$\frac{\partial z}{\partial t} + v_s\left[1 - \frac{2z}{z_{\max}}\right]\frac{\partial z}{\partial x} = q_{ls}/p \quad (21)$$

Under the assumption of steady but nonuniform clear water flow, the first term on the left hand side of equation (20) will disappear. In the case of steady and uniform clear water flow, one only needs to employ equation (21). In this case, the interaction between flow in the streamflow layer and sediment transport in the moving bed layer is interlinked through the sediment particle velocity.

[18] Model parameters basically consist of C_z, p, S_o, κ, $z_{\max}$, ρ_s and d_s. Parameters d_s and ρ_s can be obtained from experimental sediment data, while S_o, C_z, and p can be obtained from field measurements. *Ching and Cheng* [1964] suggest $\kappa = 0.756 \times 10^{-4}$ and $p = 0.528$. *Langbein and Leopold* [1968] suggest $C_{\max} = 245$ kg/m^2 (note that $z_{\max} = C_{\max}/(p\rho_s)$). For the numerical solution of equations (12) and (13), the required initial and boundary conditions, difference equations, and numerical stability conditions are summarized in Appendix B.

3. Model Testing for Hypothetical Cases

[19] The kinematic wave model (equations (12) and (13)) was first applied to three hypothetical cases in order to examine its components. These cases were analyzed assuming the inflow hydrograph and inflow concentration at the upstream end of the channel, as shown in Figures 2a and 2b. The channel was assumed to have a 1000 m length, 20 m width, 0.0025 bed slope and a Chezy roughness coefficient $C_z = 50$ m$^{0.5}$/s. The sediment was assumed to have $\rho_s = 2650$ kg/m^3, $d_s = 0.32$ mm, $p = 0.528$, and a sediment transport capacity coefficient $\kappa = 0.000075$, which is in agreement with [*Ching and Cheng*, 1964]. Note that equations (12) and (13) are solved for finding spatial and temporal variations of the h and z variables. These equations require specification of initial flow depth and bed levels, and specification of flow depth and bed levels at the upstream end. As such, the model requires information on bed level rather than concentration. However, one can always relate concentration to bed level by equation (9) (i.e., $C_b = p\, z\, \rho_s$). In Figure 2b, $C_b = 14$ kg/m^2 corresponds to a bed level of $z = 0.01$ m and $C_b = 140$ kg/m^2 corresponds to $z = 0.10$ m of bed level.

3.1. Hypothetical Case I: Effect of Inflow Concentration

[20] Figures 3a–3d present bed profiles during the rising limb, equilibrium, recession limb, and postrecession limb of the inflow hydrograph and concentration, respectively. It is seen that bed elevation gradually increases as the inflow concentration increases at the upstream end of the channel during the rising limb of the inflow concentration (Figure 3a). This increase is more pronounced at the upstream section. For the period corresponding to the equilibrium feeding of the sediment at the upstream end

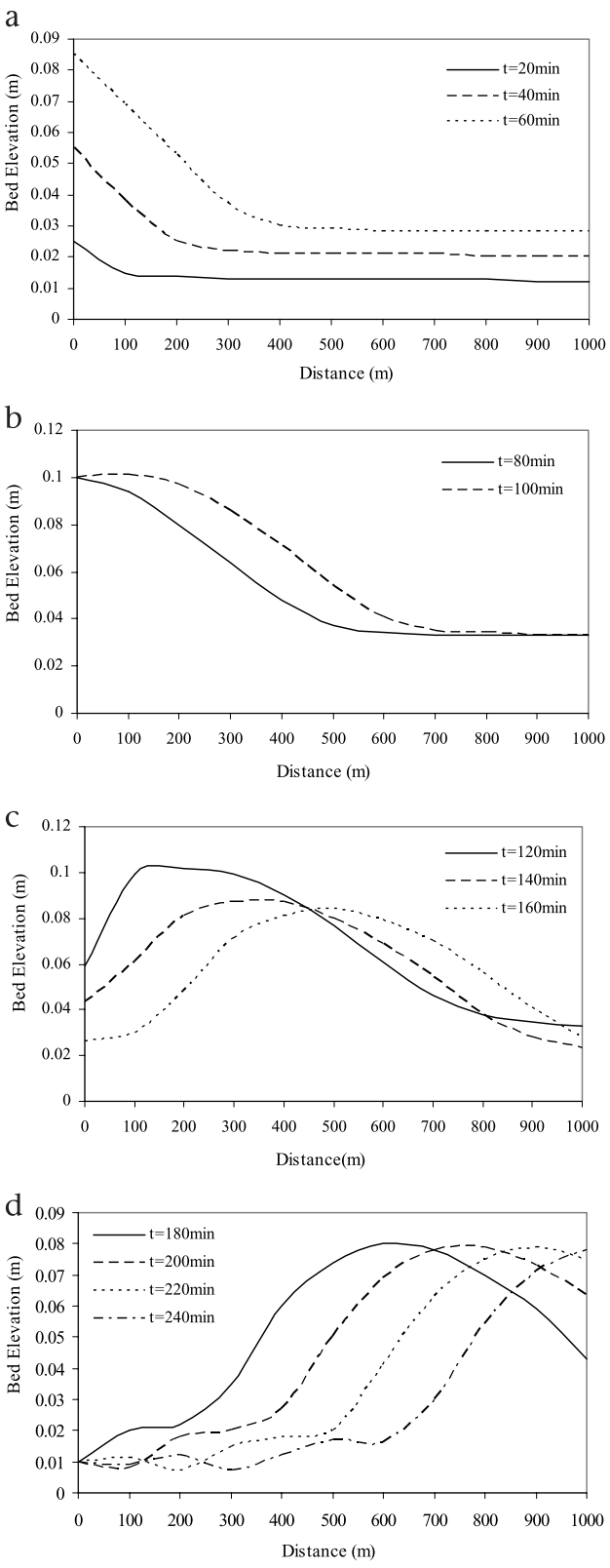

Figure 3. (a) Transient bed profile at rising period of inflow hydrograph and concentration. (b) Transient bed profile at equilibrium period of inflow hydrograph and concentration. (c) Transient bed profile at recession period of inflow hydrograph and concentration. (d) Transient bed profile at postrecession period of inflow hydrograph and concentration.

of the channel, the bed elevation continues to increase in 70% of the channel length, as shown in Figure 3b. During the recession limb of the inflow concentration, as the sediment feeding decreases the bed elevation starts to decrease toward the upstream section (in 40% of the channel length) but increases toward the downstream section (the remaining 60%) of the channel, as shown in Figure 3c. This is reasonable, since the transient bed profile moves downstream and thus concentration also increases downstream. For the postrecession period, the bed profile is shown in Figure 3d. In this case, the bed level decreases to the original level (equilibrium) at the upstream section but as time progresses it increases toward the downstream section. Thus the kinematic wave model seems to capture the expected behavior of the transient bed movement in alluvial channels, as seen from Figures 3a–3d.

3.2. Hypothetical Case II: Effect of Flow Velocity

[21] In this case, the objective was to examine the effect of flow velocity and consequently the velocity of sediment particles on the bed profile. To that end, the same inflow hydrograph (Figure 2a) but with an inflow base flow rate Q_b = 25 m^3/s and inflow equilibrium flow rate Qeq = 100 m^3/s rates, and the same sediment concentration inflow (Figure 2b) were employed. The Chezy roughness and channel width were first assumed to be 71 $m^{0.5}/s$ and 20 m, respectively, resulting in a change in the flow velocity from u = 2.5 (base flow part) to 3.97 m/s (equilibrium flow part) (case I) and then they were assumed to be 28 $m^{0.5}/s$ and 50 m, respectively, resulting in a change in flow velocity from u = 1.0 (base flow part) to 1.58 m/s (equilibrium flow part) (case II).

[22] Figures 4a–4d present transient bed profiles during the rising limb, equilibrium, recession limb, and postrecession limb of the inflow hydrograph and concentration for the two cases where at any time both cases had different flow velocities. For high velocity and sediment feeding at the upstream section, sediment particles moved downstream faster, increasing the bed elevation along the channel length, as shown in Figures 4a–4d. For example, at 40 min, under low velocity (case II) the bed wavefront moved about 300 m, while it had already reached the downstream end under high velocity (case I) (Figure 4a). In other words, under high velocity (case I), the wavefront had already passed through the downstream end (1000 m from the upstream section) and bed level at the downstream section consequently increased from a stable bed level of 0.01 m to over 0.02 m by the simulation time of 40 min (Figure 4a). At 80 min, corresponding to the equilibrium feeding of sediment at the upstream end, the bed levels close to the upstream end are almost the same but deviate toward the downstream end with higher elevation and faster speed under high velocity (Figure 4b).

[23] During the recession limb, under low velocity (case II) the bed elevation in the middle portion of the channel is higher than that under high velocity (case I). High-velocity flow moves sediment particles faster toward the downstream section, thus on the way the bed elevation reduces. On the other hand, the sediment feeding is reduced at the upstream end. Under low flow velocity sediment particles move slower, and bed elevation increases along the channel especially in the middle section. Since it takes time to reach the downstream end, the bed level is lower at that end and since the feeding reduces at the upstream end the

bed level is lower there as well (Figure 4c). This is further seen in Figure 4d corresponding to 60 min after the feeding is terminated at the upstream end. When there is no more feeding of sediment at the upstream section of the channel, the transient bed level would be expected to return to the equilibrium bed level starting from the upstream section and progressing toward the downstream of a channel. The excess sediment in time would be moved toward the downstream end and thus along the way the transient bed level would be reduced to the equilibrium bed level. Since sediment particles move slower under low velocity, it would take longer for the transient bed profile to reach the original bed level. This is seen in Figure 4d, where at the downstream end the bed elevation in case II is higher than that in case I.

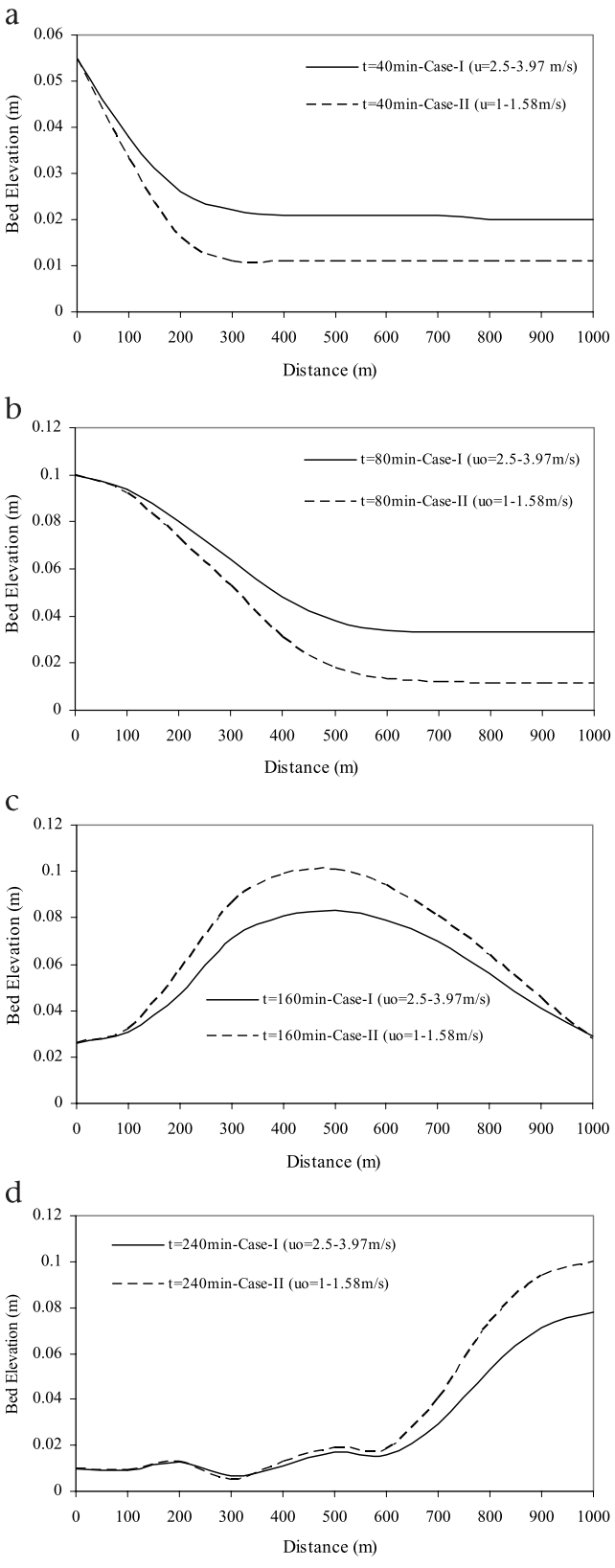

Figure 4. (a) Transient bed profile under different flow velocities at rising period of inflow hydrograph and concentration. (b) Transient bed profile under different flow velocities at equilibrium period of inflow hydrograph and concentration. (c) Transient bed profile under different flow velocities at recession period of inflow hydrograph and concentration. (d) Transient bed profile under different flow velocities at postrecession period of inflow hydrograph and concentration.

3.3. Hypothetical Case III: Effect of Maximum Concentration

[24] The objective of this case was to examine the effect of maximum concentration on transient bed profiles. For this case, the inflow hydrograph that was used for investigating the effect of flow velocity on transient bed profile was employed. The inflow concentration, shown in Figure 2b, was chosen but with an inflow base concentration C_b = 84 kg/m^2 (corresponding to bed level of z = 0.06 m) and an inflow equilibrium concentration C = 420 kg/m^2 (corresponding to bed level of z = 0.30 m). The reason for choosing different magnitudes of flow and concentration rates in the inflow hydrograph and concentration for each hypothetical case was to see whether the kinematic wave model was capable of simulating bed profiles under different flow and sediment conditions.

[25] Figures 5a–5d show the effect of maximum concentration C_{max} on transient bed profiles at different simulation times corresponding to the rising, equilibrium, recession, and postrecession periods of the inflow hydrograph and concentration. Note that equation (13) requires information on the maximum bed level (z_{max}) rather than maximum concentration (C_{max}). However, as it is stated earlier, one can relate these variables to each other by equation (9). Four different z_{max} values were chosen: 0.60, 0.45, 0.30, and 0.15 m. Note that these values correspond to concentrations of 840, 630, 420, and 210 kg/m^2, respectively. One would expect that under a greater value of z_{max} the transient bed form profile would have a higher elevation and a faster wavefront, because a greater z_{max} would allow a greater transport of sediment. This, in turn, would result in higher elevation of bed forms and sediment particles would move faster downstream. At the earlier stage of the simulation period, the bed levels increased gradually and wavefronts moved slowly (Figures 5a and 5b). At 80 min, while the front moved to 500 m under z_{max} = 0.60 m, it just reached 150 m under z_{max} = 0.15 m (Figure 5b). Similarly, at 160 min the bed wavefront moved to the downstream end under z_{max} = 0.60 m, while it just reached 400 m under z_{max} = 0.15 m (Figure 5c). This distance is 800 m for z_{max} = 0.30 m (Figure 5c). The front under z_{max} = 0.45 m closely followed

the front under z_{max} = 0.60 m for most of the simulation period (Figures 5a–5c).

[26] Sediment transport rates at various cross sections along transient bed profiles are shown in Figure 6. To that end, a constant inflow hydrograph of Q = 25 m^3/s and an excess constant inflow concentration of C = 336 kg/m^2 (corresponds to z = 0.24 m) were considered. Note that at equilibrium z = 0.06 m (corresponds to C = 84 kg/m^2) and with an excess rate it becomes $z + \Delta z$ = 0.30 m (corresponds to $C + \Delta C$ = 420 kg/m^2). The channel width was considered as 50 m and the Chezy roughness coefficient as 28 m$^{0.5}$/s. As seen in Figure 6, the sediment transport at a particular section increases rapidly from the equilibrium value, once the aggradation front reaches that section and then it gradually increases and approaches the increased sediment transport asymptotically. This result is in agreement with *Soni* [1981b].

[27] The above discussion shows that the kinematic wave model simulates moving bed profiles in alluvial channels for different hypothetical cases reasonably. In what follows, the model is tested using experimental data.

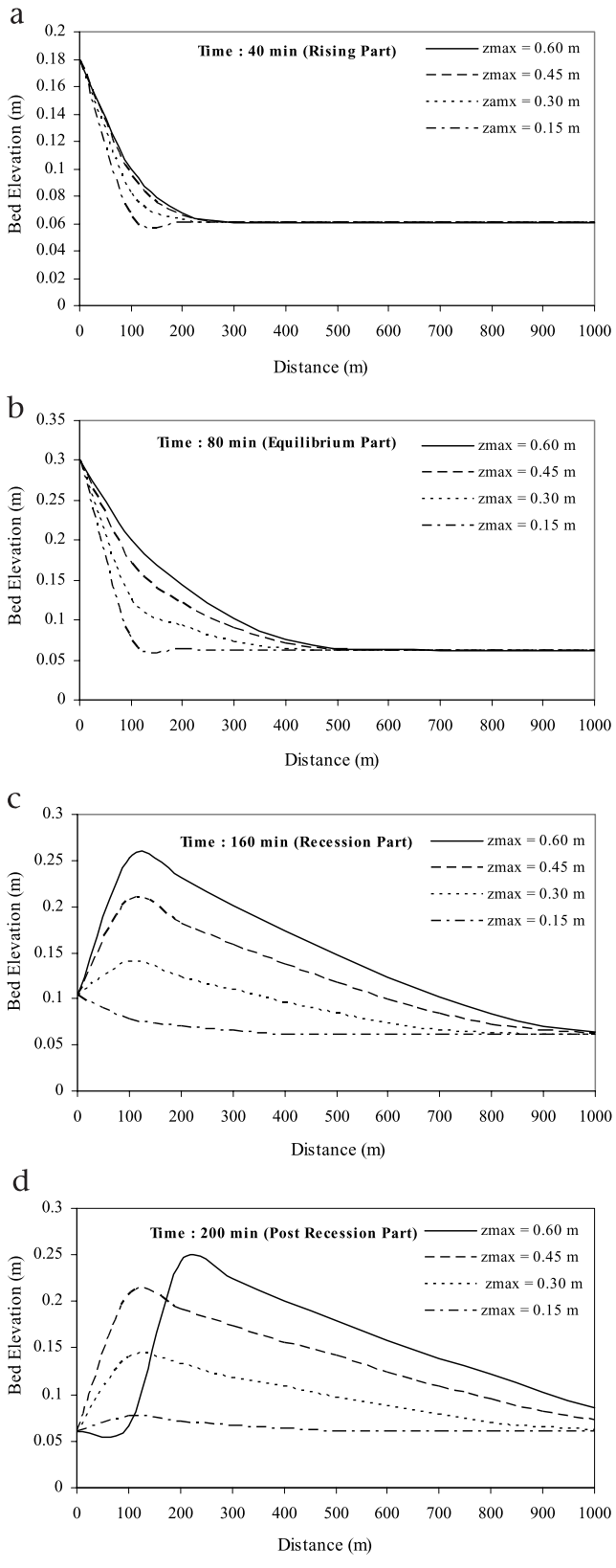

Figure 5. (a) Transient bed profile under different z_{max} values at rising period of inflow hydrograph and concentration. (b) Transient bed profile under different z_{max} values at equilibrium period of inflow hydrograph and concentration. (c) Transient bed profile under different z_{max} values at recession period of inflow hydrograph and concentration. (d) Transient bed profile under different z_{max} values at postrecession period of inflow hydrograph and concentration.

4. Model Testing Using Experimental Data

4.1. Bead Experiments

[28] The kinematic wave model was first tested against the data obtained from *Langbein and Leopold* [1968] who conducted a series of bead experiments in a 60 cm long, 7 cm wide and 5 cm high flume. They used glass spheres of 4.7 mm in diameter. The glass spheres were transported by the water flow on a smooth bed. Uniform flow depth was about 22 mm and the speed of a single bead was about 76 mm/s. They employed 11 different spacing that corresponded to different values of concentration feeding (see Table 1) at the upstream end of the flume and measured the transport rate in terms of beads per second. They obtained a flux-concentration curve from which, the average value for z_{max} was obtained as 5.5 beads per 25.4 mm (this is the same as 1 bead per diameter). The details of the experiment are given by *Langbein and Leopold* [1968].

[29] In bead experiments, there is no suspended sediment and flow is uniform and steady. Therefore it would suffice to employ equation (21) to model the bead movement and transport. Figure 7 compares predicted and measured transport rates. The model closely predicted the measured values, although it slightly underpredicted where the bead spacing was larger. For the overall performance of the model, MSE = 2.17 mm/s, $RMSE$ = 2.34 mm/s, and R^2 = 0.91, where MSE is the mean absolute error, $RMSE$ is the root mean square error, and R^2 is the coefficient of determination.

4.2. Flume Sediment Transport Experiments

[30] The kinematic wave model was tested against the experimental data of aggradation depths measured by *Soni* [1981a] in a laboratory flume of rectangular cross section. The flume was 30.0 m long, 0.20 m wide and 0.50 m deep. The flume was filled with sand to a depth of 15 cm. The sand forming the bed and the injected sediment had a median sieve diameter of d_{50} = 0.32 mm and a specific

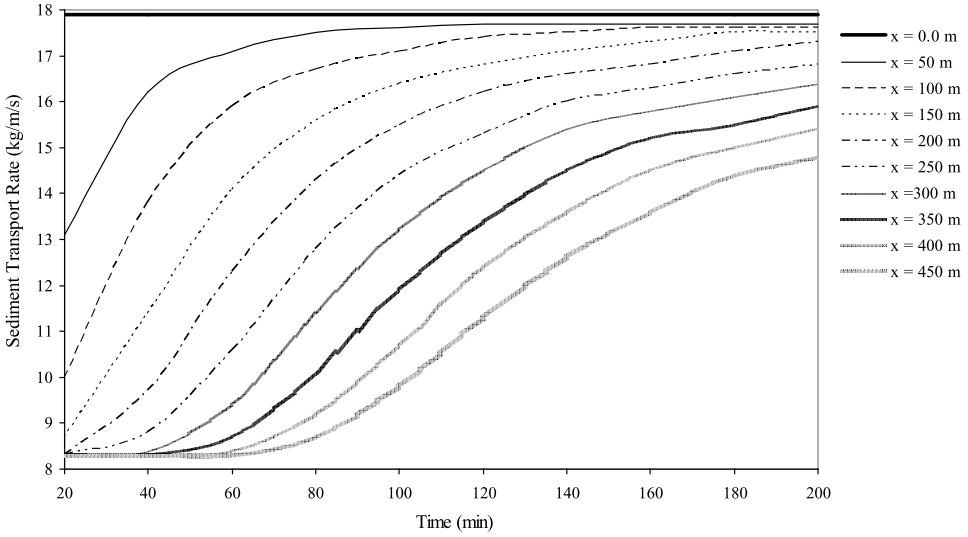

Figure 6. Variation of sediment transport rate with time and distance.

gravity of 2.65 g/cm^3. The discharge was controlled by a valve and measured by a means of calibrated orifice meter installed in the supply line. A pointer gauge mounted on a movable carriage was used to record the bed elevations.

[31] The aggradation experiments were carried out when the bed was in the mobile condition. A uniform flow was obtained by adjusting the tail gate at the downstream end of the flume allowing the bed to adjust. The concentration of sediment load was measured with a sampler at the downstream end of the flume at regular time intervals during the test run and the average equilibrium concentration was obtained. Then, the sediment was dropped manually at the upstream section at a constant rate in excess of the equilibrium concentration to cause aggradation. During aggradation, bed elevations were measured at intervals from 10 to 20 min at eleven sections. Aggradation runs were continued until the end point of the transient profiles reached the downstream end. The details of the experiment can be obtained from *Soni* [1981a].

[32] On the basis of flume sand transport experiments of *Guy et al.* [1966], *Langbein and Leopold* [1968] suggested a value of $C_{b\max} = 245$ kg/m^2. In model simulations, this value was used for computing the maximum bed elevation, $z_{\max}$. The volume of sand per unit volume of bed sediment (one minus porosity) was assumed to be $p = 0.60$. Furthermore, it was assumed that suspended sediment was negligible in accordance with *Soni* [1981a] who observed that most of the added sediment settled in the bed in a short length and then moved as a bed load. He noted that there was suspended sediment close to the section of sediment injection which was located near the upstream end of the flume. The flow was uniform and steady and suspended sediment was negligible in this experiment. Therefore equation (21) would suffice to model the bed aggradation.

[33] Figures 8a–8c show, respectively, simulations of bed profiles measured at 30, 60 and 90 min during the experimental run which had Q_{weq}=0.02 m^3/s (equilibrium flow discharge); $q_{seq} = 111 \times 10^{-6}$ m^2/s (equilibrium sediment discharge); $S_o = 0.00212$ (bed slope); $h_o = 0.092$ m (uniform flow depth) and an excess sediment rate of $\Delta q_s = 0.9 q_{seq}$. At each time, the model satisfactorily simulated the measured data. The earlier parts of the transient profiles were closely captured by the model. In simulations at 60 min and 90 min, the model-predicted transient profiles were faster than those of the measured ones in reaching the equilibrium bed profile (Figures 8b and 8c). The overall computed error measures for simulations in Figure 8 are *MSE* = 0.48 cm, *RMSE* = 0.62 cm and $R^2 = 0.98$ (Table 2).

[34] Figures 9a–9d present, respectively, simulations of bed profiles measured at 15, 45, 75 and 105 min during the

Table 1. Summary of Data on Bead Experiment[a]

Mean Linear Concentration, bead/cm	Spacing, cm	Speed of Beads, cm/s
1.02	0.99	4.27
0.98	1.02	3.36
0.87	1.17	3.97
0.79	1.27	5.09
0.66	1.52	5.64
0.49	2.03	6.10
0.35	2.79	6.56
0.33	3.05	6.71
0.29	3.43	6.41
0.20	5.08	7.17
0.15	6.60	7.63

[a]*Langbein and Leopold* [1968].

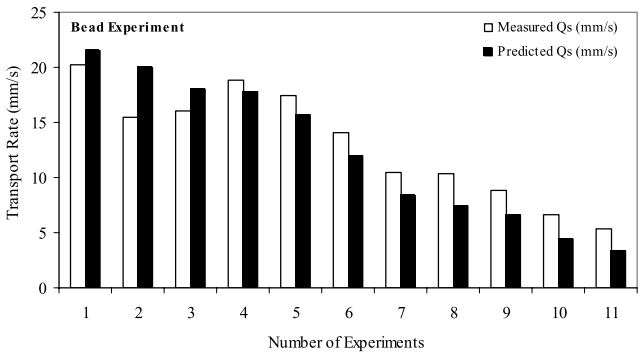

Figure 7. Comparison of model predictions with measured transport rate data (transport rate (mm/s) is in terms of "beads/second").

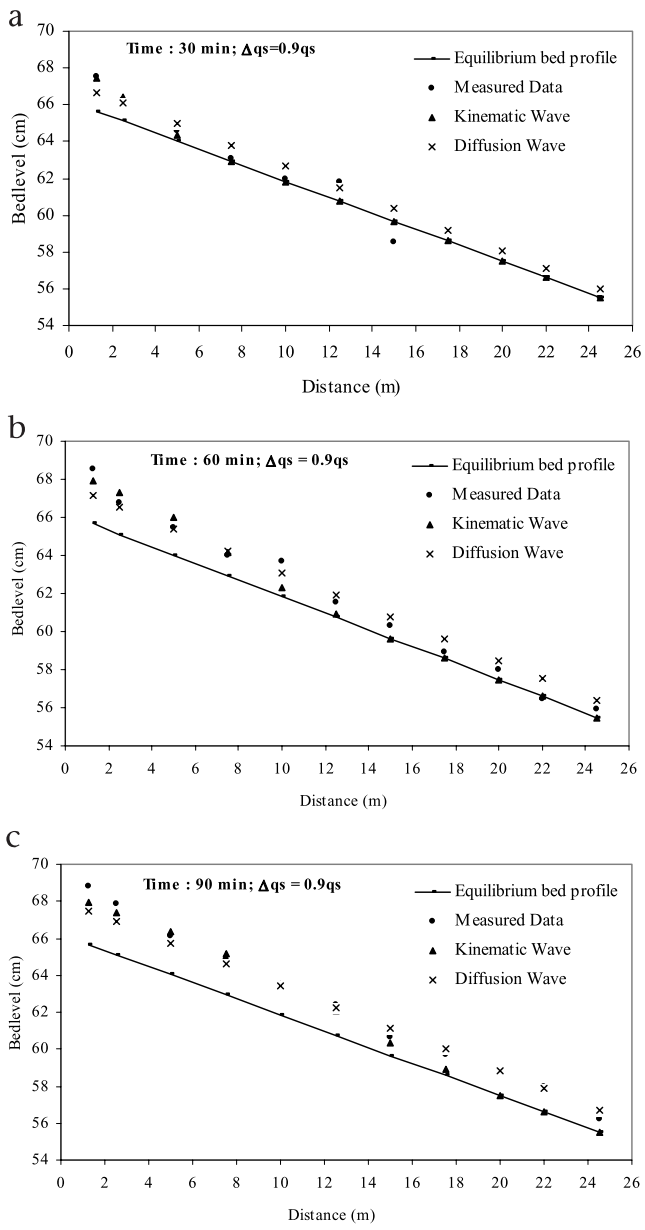

Figure 8. (a) Simulation of measured bed profile at 30 min. (b) Simulation of measured bed profile at 60 min. (c) Simulation of measured bed profile at 90 min.

experimental run that had an excess sediment rate of Δq_s = 1.35 q_{seq}. The measured data fluctuated around the equilibrium bed profile. This fluctuation was more pronounced at the earlier stages of the experiment (Figure 9a). The systematic way in which the actual data points fluctuated was due to the presence of small ripples/dunes on the bed during the course of aggradation [*Soni*, 1981a]. Furthermore, *Soni* [1981b] reported that some error in the measurements

Table 2. Error Measures[a]

	MSE, cm		RMSE, cm		R^2	
Experiment	KW	DW	KW	DW	KW	DW
$\Delta q_s = 0.9 q_{seq}$	0.48	0.52	0.62	0.66	0.98	0.96
$\Delta q_s = 1.35\ q_{seq}$	0.64	1.11	0.76	1.31	0.94	0.86

[a]KW, kinematic wave; DW, diffusion wave (analytical solution).

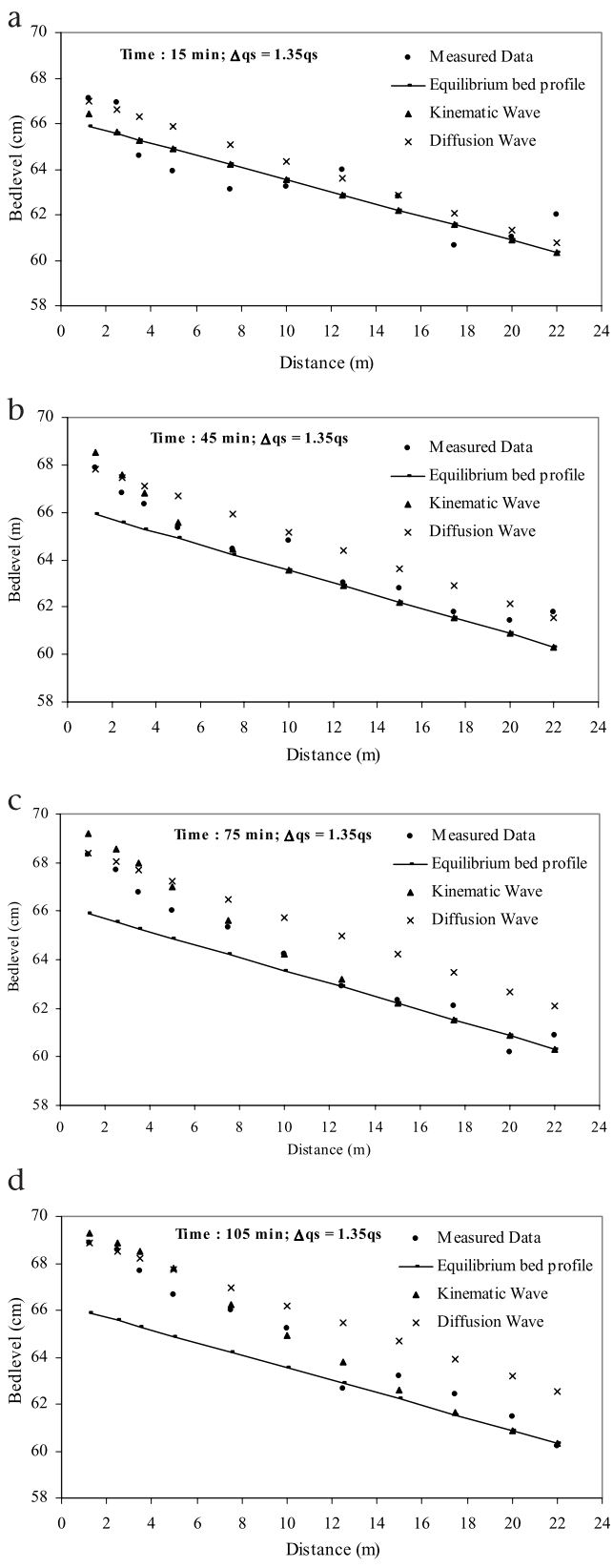

Figure 9. (a) Simulation of measured bed profile at 15 min. (b) Simulation of measured bed profile at 45 min. (c) Simulation of measured bed profile at 75 min. (d) Simulation of measured bed profile at 105 min.

toward the tail end of the transient bed profile might have occurred because of very small depositional depth profiles. This may explain the fluctuating measured data toward the end of flume at 45 and 75 min (Figures 9b and 9c). The model simulations of the transient bed profiles at 45, 75, and 105 min were satisfactory. At 45 min, the measured and predicted profiles moved very closely toward the downstream end and reached the equilibrium bed profile at the same time (Figure 9b). At 75 min, the model slightly overestimated the earlier part of the measured transient profile, yet both the measured and predicted profiles moved together and reached the equilibrium bed profile at the same time (Figure 9c). At 105 min, the predicted profile reached the equilibrium bed profile slightly earlier than did the measured one (Figure 9d). The overall computed error measures for simulations in Figure 9 are MSE = 0.64 cm, $RMSE$ = 0.76 cm and R^2 = 0.94 (Table 2). Note that slightly higher values of error measures of MSE and $RMSE$ might be due to measurement errors that caused fluctuations, especially at 15 min (Figure 9a).

5. Model Testing Against the Diffusion Wave

[35] The kinematic wave model was also tested against the commonly employed diffusion wave (*DW*) model. *de Vries* [1973] developed the following *DW* model for determination of bed transients in alluvial channels:

$$\frac{\partial z}{\partial t} - D\frac{\partial^2 z}{\partial x^2} = 0 \tag{22}$$

where D is the diffusion coefficient (L^2/T).

[36] The analytical solution of equation (22), subjected to initial condition of $z(x, 0) = 0.0$ and upstream boundary condition of $z(0, t) = z_o$, is given as [*Vreugdenhil and de Vries*, 1973; *Soni*, 1981b]:

$$z = z_o \; erfc\left(-\frac{x}{2\sqrt{Dt}}\right) \tag{23}$$

where *erfc* (.) is the complementary error function and it is, for any arbitrary variable y, defined as [*Vreugdenhil and de Vries*, 1973]:

$$erfc(y) = \frac{2}{\sqrt{\pi}}\int_y^\infty e^{-\xi^2} d\xi \tag{24}$$

The diffusion coefficient is expressed as [*Soni*, 1981b]:

$$D = \frac{bq_{bs}}{3S_o p} \tag{25}$$

where b is a coefficient and *Soni* [1981b] suggests b = 5.0. Taking the shape of the transient bed profile given by equation (23), the behavior of variation of z_o with time is determined by *Soni* [1975] as:

$$z_o = \frac{\sqrt{\pi}\Delta q_{bs} t}{2p\sqrt{Dt}} \tag{26}$$

The analytical solution given by equations (23) to (26) was applied to simulate the experimental data of *Soni* [1981a]. The model simulations are given in Figures 8a–8c and 9a–9d and the related error measures are summarized in Table 2.

[37] As seen in Figures 8a–8c and 9a–9d, although the performance of both the models (*KW* and *DW*) are comparable for simulating measured data from experiment 1 (where $\Delta q_s = 0.9 q_{seq}$), *KW* outperformed *DW* in predicting measured data from experiment 2 (where $\Delta q_s = 1.35 q_{seq}$). Analytical solutions deviated from the measured data, especially for the measured data at 45, 75, and 105 min (Figures 9a–9d) and thus it yielded errors larger than the *KW* solution (Table 2).

6. Concluding Remarks

[38] Analysis of experimental data on bead, sand, and gravel movement in flumes, pipes, and streams by *Langbein and Leopold* [1968] provided strong evidence that the evolution and movement of bed profiles can be described by the kinematic wave theory employing a functional relation between sediment transport rate and sediment concentration. Following the conceptual discussion of *Langbein and Leopold* [1968], this study developed a mathematical model based on the kinematic wave theory for simulating evolution of bed profiles in alluvial channels. Satisfactory simulations of experimental data of bead and sand movement in flumes by the developed model allude to the plausibility of the kinematic wave (KW) theory.

[39] Theoretically reasonable simulations of transient bed profiles for several hypothetical cases involving different water flow and sediment concentration characteristics further confirm that the developed KW model can be employed in simulating evolution of bed form in alluvial channels.

[40] The developed KW theory model employed Chezy's relation for relating flow velocity to flow depth (equation (3)), *Velikanov*'s [1954] relation for relating sediment concentration to flow variables (equation (5)), and the functional relation between sediment transport rate and sediment concentration (equation (7)) proposed by *Langbein and Leopold* [1968]. Satisfactory performance of the model in simulating measured data lends credence that these employed relations have potential in simulating transmission of sediment waves in alluvial channels.

[41] The results of model sensitivity reveal that the mean particle velocity and maximum concentration (maximum bed form elevation) strongly affect transient bed profiles. The comparative study in simulating measured flume data showed that the developed kinematic wave model outperformed the diffusion wave model.

[42] It should be noted that the available experimental data used to test the kinematic wave model are from uniform and steady water flow experiments with negligible suspended sediment concentration. It would be, therefore, beneficial to test the model against nonuniform and unsteady transport processes, especially the data collected in the field.

Appendix A: Particle Velocity Equation Developed by *Bridge and Dominic* [1984] and Particle Fall (Terminal) Velocity Equation Developed by *Dietrich* [1982]

[43] *Bridge and Dominic* [1984], through a theoretical consideration of the dynamics of bed load motion, developed the following expression for grain velocity:

$$v_s = \delta\left(u_* - u_{*_c}\right) \tag{A1}$$

where δ is defined as:

$$\delta = \frac{1}{K}\ln\left(\frac{y_n}{y_1}\right) \tag{A2}$$

where K = von Karman constant; y_n = distance from the boundary of effective fluid thrust on bed load grain; and y_1 = roughness height. The average value of δ is between 8 and 12 [*Bridge and Dominic*, 1984]. This study employed the value of δ = 10. u_{*c} = critical shear velocity (shear velocity at the incipient motion) and it is defined as [*Bridge and Dominic*, 1984]:

$$u_{*c} = \frac{v_f(\tan\phi)^2}{\delta} \tag{A3}$$

where tanφ is the dynamic friction coefficient and it has an average value between 0.48 and 0.58 [*Bridge and Dominic*, 1984]. This study employed a value of tanφ = 0.53. As seen in equation (A3), the critical shear velocity is a function of particle fall velocity. Analyzing a wide range of empirical data, *Dietrich* [1982] developed the following equation for particle fall velocity [*Dietrich*, 1982; *Bridge and Bennett*, 1992]:

$$W_* = R_3 10^{(R_1+R_2)} \tag{A4}$$

where

$$R_1 = -3.767 + 1.929\left(\log D_*\right) - 0.0982\left(\log D_*\right)^2 - 0.00575\left(\log D_*\right)^3 + 0.00056\left(\log D_*\right)^4 \tag{A5}$$

$$R_2 = \log\left[1 - \frac{(1-CSF)}{0.85}\right] - (1-CSF)^{2.3}\tanh\left[\log D_* - 4.6\right] + 0.3(0.5-CSF)(1-CSF)^2\left(\log D_* - 4.6\right) \tag{A6}$$

$$R_3 = \left[0.65 - \left(\frac{CSF}{2.83}\tanh\left[\log D_* - 4.6\right]\right)\right]^{\left[1+\frac{(3.5-P)}{2.5}\right]} \tag{A7}$$

where the dimensionless settling (fall) velocity of the particle (W_*) is expressed as [*Dietrich*, 1982]:

$$W_* = \frac{\rho v_f^3}{(\rho_s-\rho)g\nu} \tag{A8}$$

where ρ is the fluid (water) density. The dimensionless particle size (D_*) is expressed as [*Dietrich*, 1982]:

$$D_* = \frac{(\rho_s-\rho)g d_s^3}{\rho\nu^2} \tag{A9}$$

The Corey shape factor (*CSF*) is defined as [*Dietrich*, 1982]:

$$CSF = \frac{c}{(ab)^{0.5}} \tag{A10}$$

where a, b, and c are the longest, intermediate, and shortest axes of the particle, respectively, and are mutually perpendicular. The mean value of *CSF* for most naturally occurring sediment is between 0.5 and 0.8 [*Dietrich*, 1982]. This study employed a value of *CSF* = 0.65. P is the Powers value of roundness that has an average value between 3.5 and 6 [*Dietrich*, 1982]. This study employed the value of P = 4.75.

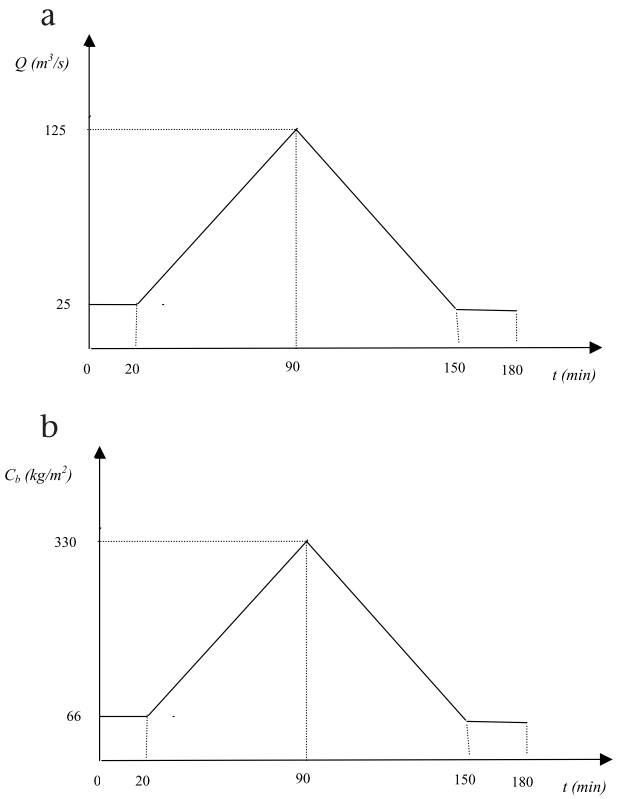

Figure A1. (a) Inflow hydrograph. (b) Inflow concentration.

Note that equation (A4) considers the influence of grain shape as well as density and size on the fall velocity of a particle.

[44] Equations (14) and (18) were used for computing the particle velocity and particle fall velocity, respectively, for the developed model (formulation I). The results of application of the model using these equations were presented above. As presented in this appendix, equations (A1) and (A4), as alternative to equations (14) and (18), can be employed for computing the particle velocity and particle fall velocity, respectively (formulation II). In order to compare both formulations, we considered a hypothetical channel having a length of 1000 m, width of 50 m and a slope of 0.0015, subjected to the inflow hydrograph and inflow sediment concentration at the upstream end, as shown in Figure A1. The Chezy roughness coefficient is assumed to be C_z = 36.5 $m^{0.5}/s$ for this channel. Figure A2 shows two simulations of bed profile along the channel length at 80 and 130 min that correspond to the rising and recession periods of the inflow hydrograph and concentration. As seen, both formulations yielded comparable results. This implies that both the formulations can be employed in modeling bed profiles using the kinematic wave model.

Appendix B: Initial, Boundary, and Numerical Stability Conditions and the Difference Equations

[45] For numerical solution of equations (12) and (13), initial and boundary conditions are needed. Initial conditions can be specified as:

$$h(x,t) = h_o, \quad t = 0.0 \tag{B1a}$$

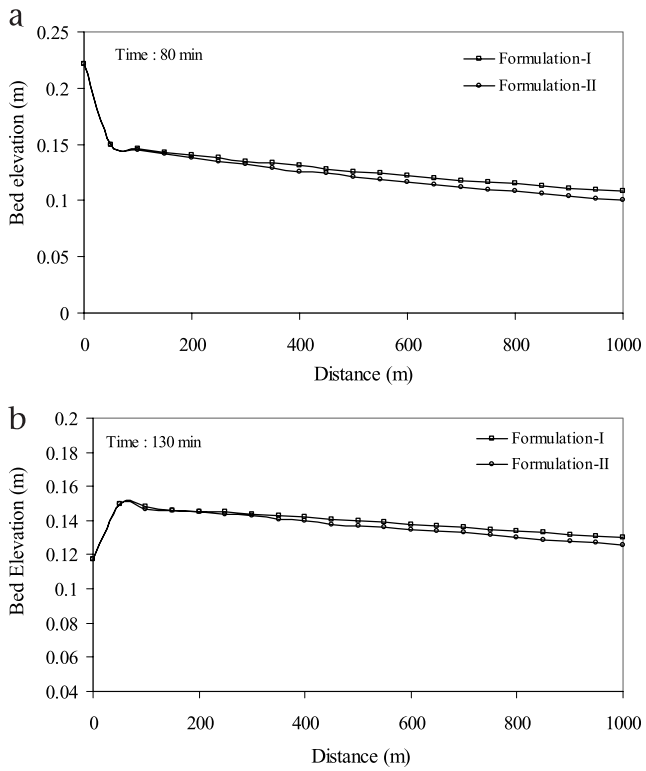

Figure A2. (a) Comparison of formulation I and formulation II for simulating bed profiles at rising period of inflow hydrograph and concentration. (b) Comparison of formulation I and formulation II for simulating bed profiles at recession period of inflow hydrograph and concentration.

$$z(x,t) = z_o, \quad t = 0.0 \tag{B1b}$$

where h_o and z_o are the initial flow depth (L), and the bed-level elevation (L), respectively.

[46] The upstream boundary conditions can be specified as inflow hydrograph (or flow depth) and inflow sediment graph (or concentration):

$$h(0,t) = h(t), \quad t > 0.0 \tag{B2a}$$

$$z(0,t) = z(t), \quad t > 0.0 \tag{B2b}$$

[47] Equations (12) and (13) are solved numerically using an explicit finite difference method. Difference equations for both layers are written not only at the central nodes of the domain but also at the downstream node. Both equations are solved simultaneously for each time step. The related difference equations are given as follows:

$$\left[1-\eta\beta\alpha^3 h_{ij}^{\beta-1}\right]\frac{\left(h_i^{j+1}-h_i^j\right)}{\Delta t}+\left[\alpha\beta h_{ij}^{\beta-1}-\eta\beta\alpha^4 h_{ij}^{2\beta-2}\right]\cdot\frac{\left(h_{i+1}^j-h_{i-1}^j\right)}{2\Delta x}+(1-p)\frac{\left(z_i^{j+1}-z_i^j\right)}{\Delta t}=q_{lw} \tag{B3a}$$

$$\left[\eta\beta\alpha^3 h_{ij}^{\beta-1}\right]\frac{\left(h_i^{j+1}-h_i^j\right)}{\Delta t}+\left[\eta(2\beta-1)\alpha^4 h_{ij}^{2\beta-2}\right]\cdot\frac{\left(h_{i+1}^j-h_{i-1}^j\right)}{2\Delta x}+p\frac{\left(z_i^{j+1}-z_i^j\right)}{\Delta t}+pv_s\left[1-\frac{2z_i^j}{z_{\max}}\right]\cdot\frac{\left(z_{i+1}^j-z_{i-1}^j\right)}{2\Delta x}=q_{ls} \tag{B3b}$$

where i stands for space node while j stands for time node. Δt and Δx are time and space increments, respectively. Note that in equations (24a) and (24b), the unknowns are the variables at time node (j + 1) (future time). Variables at time node j (the present time) are already known. For the numerical scheme, the stability conditions are found to be as:

$$\frac{v_s\Delta t}{2\Delta x} \le 0.15 \tag{B4a}$$

$$\frac{\alpha\beta\Delta t}{2\Delta x} \le 0.020 \tag{B4b}$$

Notation

a, b, and c	longest, intermediate, and shortest axis of particle.
c	volumetric sediment concentration in the water flow phase (in suspension) (L^3/L^3).
c_b	base concentration.
c_{eq}	equilibrium concentration.
C_b	areal sediment concentration (M/L^2).
$C_{b\max}$	maximum areal sediment concentration when transport ceases (M/L^2).
CSF	Corey shape factor.
C_z	Chezy roughness coefficient ($L^{0.5}/T$).
D	diffusion coefficient (L^2/T).
d_s	particle diameter (L).
g	gravitational acceleration (L/T^2).
h	flow depth (L).
K	von Karman constant.
q_{bw}	water flux in the mobile bed layer (L^2/T).
q_{ls}	lateral sediment flux (L/T).
q_{lw}	lateral water flux (L/T).
q_{sb}	sediment flux in the movable bed layer (L^2/T).
q_{st}	sediment transport rate ($M/L/T$).
Q_b	base flow rate.
Qeq	equilibrium flow rate.
p	volume of solids in unit volume of bed sediment (porosity) (L^3/L^3).
P	Powers value of roundness.
S_f	friction slope.
S_o	bed slope.
t	independent variable of time (T).
$\tan\varphi$	dynamic friction coefficient.
u	flow velocity (L/T).
u_c	critical flow velocity at the incipient sediment motion (L/T).
v_f	average fall velocity of sediments (L/T).
v_s	velocity of sediment particles as concentration approaches zero (L/T).

W_* dimensionless settling (fall) velocity of the particle.
x independent variable representing the coordinate in flow direction (L).
y_n distance from the boundary of effective fluid thrust on bed load grain.
y_1 roughness height.
z mobile bed layer elevation (L).
z_{max} maximum bed elevation (L).
α depth discharge coefficient or the kinematic wave resistance parameter ($L^{0.5}/T$).
β exponent.
δ, η, and ξ exponents that are functions of fluid and sediment characteristics.
κ coefficient of sediment transport capacity.
υ kinematic viscosity of water (L^2/T).
ρ fluid (water) density (M/L^3).
ρ_s sediment mass density (M/L^3).

References

Blatch, N. S. (1906), Works for the purification of the water supply of Washington, D. C., *Am. Soc. Civ. Eng. Trans.*, *57*, 400–408.

Bridge, J. S., and S. J. Bennett (1992), A model for the entrainment and transport of sediment grains of mixed sizes, shapes, and densities, *Water Resour. Res.*, *28*(2), 337–363.

Bridge, J. S., and D. F. Dominic (1984), Bed load grain velocities and sediment transport rates, *Water Resour. Res.*, *20*(4), 476–490.

Cao, Z., and P. A. Carling (2003), On evolution of bed material waves in alluvial rivers, *Earth Surf. Processes Landforms*, *28*, 437–441.

Chien, N., and Z. H. Wan (1999), *Mechanics of Sediment Transport*, Am. Soc. of Civ. Eng., Reston. Va.

Ching, H. H., and C. P. Cheng (1964), Study of river bed degradation and aggradation by the method of characteristics, *Chin. J. Hydraul. Eng.*, *5*, 1–54.

Cui, Y., and G. Parker (2005), Numerical model of sediment pulses and sediment-supply disturbances in mountain rivers, *J. Hydraul. Eng.*, *131*(8), 646–656.

Cui, Y., G. Parker, T. E. Lisle, J. Gott, M. E. Hansler-Ball, J. E. Pizzuto, N. E. Allmendinger, and J. M. Reed (2003a), Sediment pulses in mountain rivers: 1. Experiments, *Water Resour. Res.*, *39*(9), 1239, doi:10.1029/2002WR001803.

Cui, Y., G. Parker, J. Pizzuto, and T. E. Lisle (2003b), Sediment pulses in mountain rivers: 2. Comparison between experiments and numerical predictions, *Water Resour. Res.*, *39*(9), 1240, doi:10.1029/2002WR001805.

Cui, Y., G. Parker, T. E. Lisle, J. E. Pizzuto, and A. M. Dodd (2005), More on the evolution of bed material waves in alluvial rivers, *Earth Surf. Processes Landforms*, *30*, 107–114.

de Vries, M. (1965), Consideration about non-steady bed-load transport in open channels, paper presented at XI Congress, Int. Assoc. of Hydraul. Eng. and Res., St. Petersburg, Russia.

de Vries, M. (1973), River bed variation—Aggradation and degradation, *Publ. 107*, Delft Hydaulic Lab., Delft, Netherlands.

Dietrich, W. E. (1982), Settling velocity of natural particles, *Water Resour. Res.*, *18*(6), 1615–1626.

Durand, R. (1953), Basic relationships of the transportation of solids in pipes, paper presented at International Hydraulics Convention, St. Anthony Falls Hydraul. Lab., Minneapolis, Minn.

Gomez, B., and M. Church (1989), An assessment of bed load sediment transport formulae for gravel bed rivers, *Water Resour. Res.*, *25*(6), 1161–1186.

Gongcharov, B. N. (1962), *River Dynamics*, Hydrol. and Morphol. Press, St. Petersburg, Russia.

Guy, H. P., D. B. Simons, and E. V. Richardson (1966), Summary of alluvial channel data from flume experiments, 1956–1961, *U.S. Geol. Surv. Prof. Pap.*, *462–I*, 96 pp.

Hotchkiss, R. H., and G. Parker (1991), Shock fitting of aggradational profiles due to backwater, *J. Hydraul. Eng.*, *117*(9), 1129–1144.

Howard, G. W. (1939), Transportation of sand and gravel in a 4–inch pipe, *Am. Soc. Civil Eng. Trans.*, *104*, 1334–1380.

Lai, C.-T. (1991), Modeling alluvial-channel flow by multimode characteristic method, *J. Eng. Mech.*, *117*, 32–53.

Langbein, W. B., and L. B. Leopold (1968), River channel bars and dunes—Theory of kinematic waves, *U.S. Geol. Surv. Prof. Pap.*, *422–L*, 20 pp.

Levy, I. I. (1957), *River Dynamics*, Natl. Energy Resour. Press, Moscow, Russia.

Lisle, T. E., J. E. Pizzuto, H. Ikeda, F. Iseya, and Y. Kodama (1997), Evolution of a sediment wave in an experimental channel, *Water Resour. Res.*, *33*, 1971–1981.

Lisle, T. E., Y. T. Cui, G. Parker, J. E. Pizzuto, and A. M. Dodd (2001), The dominance of dispersion in the evolution of bed material waves in gravel-bed rivers, *Earth Surf. Processes Landforms*, *26*, 1409–1420.

Mahmood, K. (1975), Mathematical modeling of morphological transients in sandbed canals, paper presented at 16th Congress, Int. Assoc. of Hydraul. and Eng. Res., Sao Paulo, Brazil.

Phillips, B. C., and A. J. Sutherland (1983), Mathematical modeling of lag effects in bed load transport, paper presented at 8th Australian Fluid Mechanics Conference, Univ. of Newcastle, Newcastle, N. S. W., Australia, 28 Nov. to 2 Dec.

Pianese, D. (1994), Comparison of different mathematical models for river dynamics analysis, paper presented at International Workshop on Floods and Inundations related to Large Earth Movements, Trent Univ., Trent, Italy, 4–7 Oct.

Ribberink, J. S., and J. T. M. Van Der Sande (1985), Aggradation in rivers due to overloading—Analytical approaches, *J. Hydraul. Res.*, *23*(3), 273–283.

Rouse, H. (1938), *Fluid Mechanics for Hydraulic Engineers*, chap. XI, Dover, Mineola, N. Y.

Sharmov, G. I. (1959), *River Sedimentation*, Hydrol. and Morphol. Press, St. Petersburg, Russia.

Singh, V. P. (1996), *Kinematic Wave Modeling in Water Resources: Surface Water Hydrology*, John Wiley, Hoboken, N. J.

Soni, J. P. (1975), Aggradation in streams due to increase in sediment load, Ph.D. thesis, Univ. of Roorkee, Roorkee, India.

Soni, J. P. (1981a), Laboratory study of aggradation in alluvial channels, *J. Hydrol.*, *49*, 87–106.

Soni, J. P. (1981b), An error function solution of sediment transport in aggradation channels, *J. Hydrol.*, *49*, 107–119.

Velikanov, M. A. (1954), Gravitational theory of sediment transport (in Russian), *J. Sci. Soviet Union*, *4*.

Vreugdenhil, C. B., and M. de Vries (1973), Analytical approaches to non-steady bedload transport, *Res. Rep., S 78*, part IV, 16 pp., Delft Hydaul. Lab., Delft, Netherlands.

Wathen, S. J., and T. B. Hoey (1998), Morphological controls on the downstream passage of a sediment wave in a gravel-bed stream, *Earth Surf. Processes Landforms*, *23*, 715–730.

Yang, C. T. (1996), *Sediment Transport Theory and Practice*, McGraw-Hill, New York.

Yang, C. T., and S. Wan (1991), Comparison of selected bed-material load formulas, *J. Hydraul. Eng.*, *117*(8), 973–989.

V. P. Singh, Department of Biological and Agricultural Engineering, Texas A & M University, Scoates Hall, 2117 TAMU, College Station, TX 77843-2117, USA. (vsingh@tamu.edu)

G. Tayfur, Department of Civil Engineering, Izmir Institute of Technology, Gulbahce Kampus, Urla, Izmir, 35340, Turkey. (gokmentayfur@iyte.edu.tr)